IEEE Access
Multidisciplinary : Rapid Review : Open Access Journal

Received March 10, 2020, accepted April 4, 2020, date of publication April 10, 2020, date of current version April 29, 2020.

Digital Object Identifier 10.1109/ACCESS.2020.2987098

An Improved Droop Control for Balancing State of Charge of Battery Energy Storage Systems in AC Microgrid

DEMIN LI[1], (Graduate Student Member, IEEE), ZAIJUN WU[1], (Member, IEEE), BO ZHAO[2], (Member, IEEE), AND LEIQI ZHANG[2], (Member, IEEE)
[1]School of Electrical Engineering, Southeast University, Nanjing 210096, China
[2]State Grid Zhejiang Electric Power Research Institute, Hangzhou 310014, China

Corresponding author: Zaijun Wu (zjwu@seu.edu.cn)

This work was supported by the National Natural Science Foundation of China under Award 51877039.

ABSTRACT In order to avoid overuse of a certain battery energy storage system (BESS) and prolong the cycle life of battery in AC microgrid, an improved SoC-based droop control based on multi-agent system (MAS) is proposed for achieving State of Charge (SoC) balance of multiple BESS units. A proportional-integral (PI) adjustment item using the average SoC is added to the P-f droop to regulate the charging and discharging power of BESS, then SoC changes towards in the direction of consistency and finally reaches equalization. The dynamic average consensus algorithm is utilized to obtain the average SoC. The proposed SoC-based droop method needs not to be changed in different operating mode of BESS and can achieve SoC balance regardless of whether the capacities of different batteries are the same, which improve the applicability of this method. A complete small-signal state space model including all BESS units is built and analyzed to select the appropriate control parameters of the improved droop. The impact of communication time delay on the improved droop method for balancing SoC is investigated and the effectiveness of the proposed strategy is verified through the simulation results of different case studies.

INDEX TERMS BESS, SoC-based droop control, SoC balance, small-signal state space model.

I. INTRODUCTION

Aiming at reducing greenhouse gas emissions for facing the challenges of serious environmental pollution, various measures including using renewable energy sources (RESs) such as wind turbine (WT) and photovoltaic (PV) for power generation are adopted. Although wind and solar energy are inexhaustible to provide clean energy, they change with the variation of weather, resulting in the output power of RESs to be random, intermittent, and fluctuating [1]. Problems such as deterioration of power quality and system stability arise when large scales of RESs are connected to power grid. Therefore, U.S. Department of Energy proposed to construct Microgrid for integrating RESs, energy storage system (ESS) and loads instead of connecting the RESs to the power grid directly, which can mitigate the intermittent impacts of RESs on power grid since the ESS can restraint the uncertainty volatility of RESs. Furthermore, the output power of RESs in microgrid is directly supplied to the local load basically instead of first uploading to the power grid and then providing energy for load, which can promote the in-situ consumption of RESs output power.

The maximum power point tracking (MPPT) algorithm [2] is usually used by RESs, but it does not emphasize the real-time matching of RESs generation and load consumption. Both the RESs output fluctuation and load variation can cause a supply-demand imbalance in a microgrid [3]. To overcome this problem, the RESs output is reduced when renewable energy generation exceeds load demand [4], and operating load shedding when load demand exceeds the maximum RESs output [5]. However, these approaches will lower the energy usage efficiency and may cause the dissatisfaction of power users. ESS can restraint RESs output fluctuation and load variation. An AC microgrid composed of RESs, ESSs, loads and communication network is shown in Fig.1, in which battery energy storage system (BESS) consisting of battery and the control system is usually used as the backup device to maintain the power balance of supply-demand sides.

The associate editor coordinating the review of this manuscript and approving it for publication was Zheng H. Zhu.

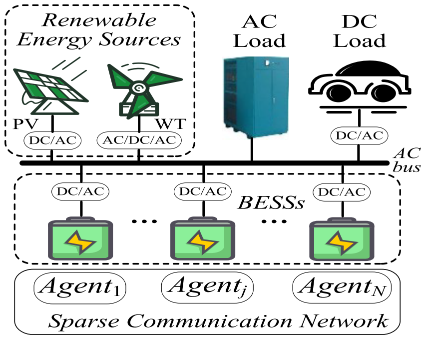

FIGURE 1. Schematic diagram of an AC microgrid including communication network.

BESS can absorb the excess power of RESs or discharge to compensate the power shortage of microgrid, which provide the microgrid with several extra values such as renewable smoothing, higher grid efficiency and improved power quality [6], [7]. Since the price of battery is still very expensive at present, the effective application of BESS is particularly important. A crucial factor to check whether the battery is in a healthy state is State of Charge (SoC), and the SoC should be maintained in a safe range for avoiding fast degradation to the battery. In [8], an autonomous active power control based on SoC and bus frequency to coordinate RES, ESS and load is presented, and the SoC of ESS can be kept in a safe limit. But the strategy does not consider the coordinated control among different ESS units. Generally, there are multiple BESS units involved in the power balancing process in microgrid. Some of them may be overcharged or over discharged if there is no control on SoC balance of BESS [9], [10]. Thus the SoC among different BESS units should be balanced to prevent overuse and uneven degradation in some of the units and prolong their service life, and this paper mainly focuses on achieving SoC balance among different BESS units.

Aiming at balancing SoC of BESS in microgrid, several major approaches are presented and mainly divided into three categories. One is centralized control [11]–[13], which requires a centralized controller to coordinate all BESS units for charging or discharging. In [11], SoC equalization can be achieved by adding a weighted factor into droop coefficient and the strategy is based on centralized control architecture in islanded AC microgrids. However, it is susceptible to single-point failures. Another is decentralized control [14]–[16]. In [14] and [15], a double-quadrant SoC-based control method to change droop coefficients are presented. The droop coefficient is proportional to the nth order of SoC in charging mode and inversely proportional to the nth order of SoC in discharging mode. However, the control method should be changed in different operating mode of BESS, which is inconvenient in practical application [16]. In [16], a rising coefficient about SoC used as an adjusting variable is added to the droop control, and then SoC changes towards consistency. The third is distributed control [17]–[20]. Multi-agent system (MAS) based on the sparse communication network provides a flexible cooperation among different BESS units without using a centralized controller [19], which improves the reliability of microgrids compared with centralized control. In [20], a frequency scheduling instead of adaptive droop gain to regulate the output of ESS is presented, in which the average SoC calculated by distributed agents is used to generate a frequency adjusting variable. Similar to [16], the variable that regulates the power output in droop control is essentially a proportional adjustment item, and it may take a long time for proportional regulator to achieve the approximate consistency of SoC.

Since distributed control allows coordination among multiple BESS units without data centralization which improves system's robustness compared with centralized control, and has more flexibility compared with fully decentralized control [21]–[23], this paper uses distributed method to balance SoC based on a sparse communication network. For an autonomous AC microgrid without central control system as shown in Fig. 1, droop control is used for BESS to provide frequency and voltage support. It is desired that a unified improved droop control strategy is adopted to control the BESS unit with higher SoC to deliver more power than others in discharging process, and to absorb less power in charging process. Meanwhile, considering that changing droop coefficient usually leads to stability issues, this paper uses frequency scheduling to modify droop control for regulating power output. If a frequency adjusting variable about SoC is added to the droop control, different BESS units can reasonably distribute their power outputs to make SoC changes in the direction of consistency. Based on the above ideas, the paper uses average SoC value to obtain the frequency adjusting variable. By extending [20], a proportional-integral (PI) adjustment item is used to modify droop control, in which the main function of the integral item is to accelerate SoC balance. Thus the improved SoC-based droop control can achieve SoC equalization rapidly and there is no need to change the control method in different operating mode of BESS.

To obtain the average SoC value, the dynamic average consensus algorithm [24]–[26] based on MAS is adopted. Each BESS unit is assigned with an agent to collect the local information and exchange them with neighboring agents to obtain the global information through a sparse communication network. Then the agent calculates average SoC value through dynamic average consensus algorithm, and generates a frequency adjusting variable to regulate the output power of local BESS. Small signal analysis is implemented to design the relevant control parameters and ensure stability of the improved SoC-based droop control. The effectiveness and advanced features of the proposed method is verified through different case studies.

The rest of this paper is organized as follows. The improved SoC-based droop control utilizing average SoC value is proposed in Section II. The control parameters of the proposed method are designed through small signal analysis in Section III. In Section IV, simulation results of different case studies are analyzed. Finally, Section V concludes this paper.

II. SoC BALANCE CONTROL USING DYNAMIC AVERAGE CONSENSUS

A. SoC BALANCE CONTROL

As mentioned above, RESs usually operate in MPPT mode to feed the load consumption, and the mismatch between RESs output and load demand is balanced by BESS using droop control. For the jth BESS unit shown in Fig. 1, the conventional P-f droop is given by

$$f_j = f_n - m_j P_{B\_j} \tag{1}$$

where f_j, m_j and P_{B_j} are the output frequency, droop coefficient of P-f and charging or discharging power of jth BESS unit, respectively. f_n is the nominal frequency.

The battery of a BESS unit is usually connected to the AC common bus via a bidirectional DC/AC converter. The output current and voltage of battery are practically the input current and voltage of its converter, then the output power of battery equals to that of converter if the power loss in the converter is omitted, i.e.,

$$p_j = p_{b\_j} = V_{b\_j} i_{b\_j} \tag{2}$$

where p_j, p_{b_j}, V_{b_j} and i_{b_j} are the output power of converter, the output power, voltage and current of battery for the jth BESS unit, respectively.

The output power of converter, i.e., p_j, is set to be negative if BESS is charging or battery absorbs power, while p_j is set to be positive if BESS is discharging or battery releases power. The SoC varies along with the charging or discharging of BESS. Since the premise of achieving SoC balance is estimating the SoC of battery, and the paper mainly focuses on balancing SoC instead of the precise SoC estimation, the common SoC estimation, which is based on the assume that all the input voltages of converters are equal [19], is used as follows

$$SoC_j = SoC_{0\_j} - \frac{\int i_{b\_j} dt}{C_{ej}} = SoC_{0\_j} - \frac{\int p_j dt}{E_j} \tag{3}$$

where SoC_{0_j} and C_{ej} are the initial value of SoC and battery capacity for the jth BESS unit, respectively. $E_j = C_{e\,j} V_{b\_j}$.

After the output power of converter passed through a low-pass filter, the fundamental component of p_j is obtained to improve power quality, thus the relationship between p_j and P_{B_j} in (1) is as follows

$$P_{B\_j} = \omega_c p_j / (s + \omega_c) \tag{4}$$

where ω_c is the cut-off frequency of the low-pass filter.

The change amount of SoC in a short period of time can be obtained based on (3), that is

$$\Delta SoC_j \approx -(p_j \Delta t)/E_j \tag{5}$$

where Δt denotes a short period of time.

Combining (4) and (5), we can see that the change amounts of SoC for all BESS units will be equal in a short period of time as long as the ratio of output power to capacity of each BESS unit is equal to that of other units, that is, if $P_{B\_1}/E_1 = P_{B\_2}/E_2 = \ldots = P_{B\_N}/E_N$, we will have $\Delta SoC_1 = \Delta SoC_2 = \ldots = \Delta SoC_N$ for N BESS units. Furthermore, the output frequencies of all BESS units operated in parallel are equal at steady state, and then $m_1 P_{B\_1} = m_2 P_{B\_2} = \ldots = m_N P_{B\_N}$ is satisfied according to (1). From the above analysis, we can deduce (6) if $P_{B\_1}/E_1 = P_{B\_2}/E_2 = \ldots = P_{B\_N}/E_N$.

$$\begin{aligned} P_{B\_1} : P_{B\_2} : \ldots : P_{B\_N} &= \frac{1}{m_1} : \frac{1}{m_2} : \ldots : \frac{1}{m_N} \\ &= E_1 : E_2 : \ldots : E_N \end{aligned} \tag{6}$$

Equation (6) shows that once the droop coefficients of P-f for all BESS units are set to be inversely proportional to their capacities, the ratio of output power to capacity of each BESS unit is equal to that of other units, and then the change amounts of SoC will be equal, i.e., $\Delta SoC_1 = \Delta SoC_2 = \ldots = \Delta SoC_N$, in a short period of time, or in other words, all SoCs change at the same rate with the regulating of (1) regardless of whether different battery capacities are equal once the droop coefficients are set to be inversely proportional to their capacities.

In order to achieve SoC balance when BESSs have different SoCs, the rates of change of different SoCs should be unequal to make all SoCs change towards consistency. From another perspective, the process of SoC balance is actually the process that different SoCs approach and reach the average SoC. Thus a proportional-integral (PI) adjustment item about the average SoC value is used to modify (1), that is

$$\begin{aligned} f_j = f_n - m_j[&P_{B\_j} - k_{mP}(SoC_j - SoC_{ave}) \\ &- k_{sj} k_{mI} \int (SoC_j - SoC_{ave}) dt] \end{aligned}$$
$$\text{where } k_{sj} = \begin{cases} 1, & \text{if } |SoC_j - SoC_{ave}| \geq d_{SoC} \\ 0, & \text{if } |SoC_j - SoC_{ave}| < d_{SoC} \end{cases} \tag{7}$$

where SoC_{ave} is the average SoC value. k_{mP} and k_{mI} are the proportional and integral parameters of the PI item, respectively. k_{sj} is a judgment signal according to the difference between SoC_j and SoC_{ave}. d_{SoC} is a very small threshold to judge whether SoC reaches SoC_{ave}. It is deemed that SoC_j reaches SoC_{ave} if the absolute value of the difference between SoC_j and SoC_{ave} is less than d_{SoC}, then k_{sj} changes from 1 to 0 and the integral item in (7) is eliminated. Meanwhile, the proportional item, i.e., $k_{mP}(SoC_j\text{-}SoC_{ave})$, is almost zero due to $|SoC_j\text{-}SoC_{ave}| < d_{SoC}$, then the PI adjustment item can be ignored. Hence, after SoC_j reaches SoC_{ave}, (7) is basically the conventional P-f droop, which is (1).

In order to explain why SoC_j can approach and reach SoC_{ave} under the regulation of (7), we assume that there exists a virtual BESS unit operated in parallel with the jth BESS unit, which is set to be the j'th BESS unit and its SoC is SoC_{ave}, i.e., $SoC'_j = SoC_{ave}$. The capacity of the j'th battery is equal to that of the jth battery, and then the droop coefficients of the two BESS units are equal, thus

$$\begin{aligned} f'_j = f_n - m_j[&P'_{B\_j} - k_{mP}(SoC'_j - SoC_{ave}) \\ &- k'_{sj} k_{mI} \int (SoC'_j - SoC_{ave}) dt] \end{aligned}$$

$$\text{where } k'_{sj} = \begin{cases} 1, & if\,|SoC'_j - SoC_{ave}| \geq d_{SoC} \\ 0, & if\,|SoC'_j - SoC_{ave}| < d_{SoC} \end{cases} \tag{8}$$

where $f'_j = f_j$ since the two units operated in parallel.

Combining (7) and (8), we have

$$P_{B\_j} - P'_{B\_j} = k_{mP}(SoC_j - SoC_{ave}) + k_{sj}k_{mI}\int (SoC_j - SoC_{ave})dt \tag{9}$$

Assuming that $SoC_j > SoC'_j$, i.e., $SoC_j > SoC_{ave}$, then P_{B_j} will be larger than P'_{B_j}. There will be $P_{B\_j} > P'_{B\_j} > 0$ in discharging state. The absolute value of ΔSoC_j is larger than that of $\Delta SoC'_j$ according to (4) and (5). Hence, SoC_j decreases faster than SoC'_j and the value of $|SoC_j\text{-}SoC'_j|$ also decreases. Until $|SoC_j\text{-}SoC'_j| < d_{SoC}$, i.e., $|SoC_j\text{-}SoC_{ave}| < d_{SoC}$, SoC_j is deemed to reach SoC'_j. Meanwhile, k_{sj} becomes zero and the PI item can be ignored, which resulting in $P_{B\_j} \approx P'_{B\_j}$. After that, they decrease at the same rate.

If the two BESS units are in charging state, there will be $0 > P_{B\_j} > P'_{B\_j}$ based on the assume that $SoC_j > SoC'_j$. The absolute value of ΔSoC_j is less than that of $\Delta SoC'_j$ according to (4) and (5). Hence, SoC_j increases more slowly than SoC'_j and the value of $|SoC_j\text{-}SoC_{ave}|$ decreases. After $|SoC_j\text{-}SoC_{ave}|$ is less than d_{SoC}, SoC_j and SoC'_j will increase at the same rate, which is like the discharging case. In other words, SoC_j will approach and reach SoC'_j regardless of the two BESS units are in charging or discharging state if $SoC_j > SoC'_j$.

Assuming that $SoC_j < SoC'_j$, i.e., $SoC_j < SoC_{ave}$, P_{B_j} will be smaller than P'_{B_j}. There will be $0 < P_{B\_j} < P'_{B\_j}$, which will cause SoC_j to decrease more slowly than SoC'_j in discharging process, or $P_{B\_j} < P'_{B\_j} < 0$, which will cause SoC_j to increase faster than SoC'_j in charging process. Similar to the case in $SoC_j > SoC'_j$, SoC_j will also approach and reach SoC'_j in the case of $SoC_j < SoC'_j$ regardless of the two BESS units are in charging or discharging state. When the different SoCs of all BESSs reach SoC_{ave}, SoC balance is achieved by using the proposed SoC-based droop control, i.e. (7). After that, the PI item in (7) is almost zero and (7) is basically (1). Then all SoCs change at the same rate.

B. DYNAMIC AVERAGE CONSENSUS ALGORITHM

In order to get the average SoC in a distributed way, a sparse communication network based on MAS is used for the agent of each BESS unit to communicate with its neighboring agents to obtain their SoC information, and then calculate the SoC_{ave} through dynamic average consensus algorithm. The dynamic average consensus algorithm executed by the agent j is as follows

$$\begin{cases} SoC_{ave\_j}(k+1) = SoC_j(k) + \alpha \sum_{l \in N_j} \gamma_{jl}(k+1) \\ \gamma_{jl}(k+1) = \gamma_{jl}(k) + SoC_{ave\_l}(k) - SoC_{ave\_j}(k) \end{cases} \tag{10}$$

where k denotes a iteration counter value. N_j represents a set of the neighboring agents that communicate with agent j, in which agent l belongs to N_j and $l \neq j$. SoC_{ave_j} is used as

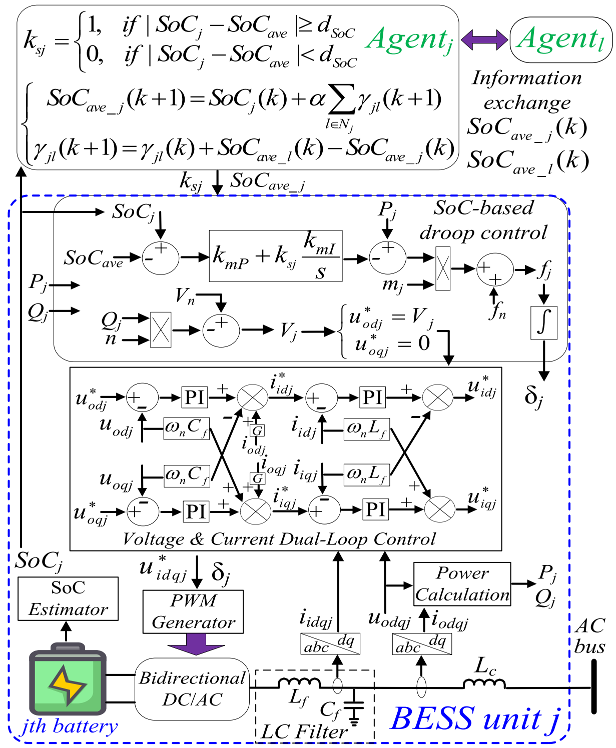

FIGURE 2. Control structure of a BESS unit.

the average SoC, i.e., SoC_{ave}, in (7) for the jth BESS unit. $\gamma_{jl}(k)$ is an additional variable for the neighbor agent l of agent j, which stores the cumulative disagreement of the two agents, and $\gamma_{jl}(0) = 0$.α is a scaling factor, which is set according to the convergence speed and stability comprehensively [20], [26]. As long as the value of α is set properly, all average SoCs can converge to a common value after a number of iterations, i.e., $SoC_{ave\_1} = SoC_{ave\_2} = \ldots = SoC_{ave\_N}$.

III. SYSTEM DESIGN METHOD

A. CONTROL PARAMETERS DESIGN OF SoC-BASED DROOP

The control structure of a BESS unit is shown in Fig. 2. The complete small signal model including all BESS units is deduced to set the control parameters of the proposed SoC-based droop properly. The jth battery is connected to common bus via a converter, a LC filter and coupling inductor which is used to remove the harmonic currents [27]. The inductance current of LC filter, output voltage and current of the jth BESS unit are converted to d-q axis voltages and currents, which are i_{idqj}, u_{odqj} and i_{odqj}, respectively. The output active and reactive power, i.e., P_j and Q_j, are obtained by using u_{odqj} and i_{odqj}, i.e.,

$$\begin{cases} P_j = \omega_c(u_{odj}i_{odj} + u_{oqj}i_{oqj})/(s+\omega_c) \\ Q_j = \omega_c(u_{odj}i_{oqj} - u_{oqj}i_{odj})/(s+\omega_c) \end{cases} \tag{11}$$

The P_j in (11) is actually the P_{B_j} in (7), which is used in the improved droop control. Q_j is used in Q-V droop control, which is $V_j = V_n\text{-}n_jQ_j$, to generate the d-axis voltage reference of voltage & current dual-loop control, i.e., $u_{odj}^{*} = V_j$. The q-axis voltage reference of voltage & current dual-loop control is zero, i.e., $u_{oqj}^{*} = 0$.n_j is the droop coefficient in Q-V, and V_n is the nominal voltage. In addition, the f_j in (7) is passed through an integrator to generate the angular of voltage reference, i.e., δ_j.

Different from using f_j to regulate P_{B_j} directly for the jth BESS unit in actual control structure, all the variables from their converter reference of each BESS unit should be convert to a common frame [28] to establish a complete small-signal state space model since there is more than one BESS unit, thus the angle difference between the jth converter reference and the common d-q frame is as follows

$$\theta_j = \int 2\pi (f_j - f_{com})dt \tag{12}$$

where f_{com} is the frequency of the common frame taken by the converter of the first BESS unit usually, i.e., $f_{com} = f_1$.

To linearize θ_j, f_j in (7) should be linearized first. f_j contains SoC_j and SoC_{ave}, in which SoC_j can be regarded as the integral of p_j and SoC_{ave} can be expressed as $(SoC_1 + SoC_2 \ldots + SoC_N)/N$ during the derivation. Thus f_j is actually an expression of p_j. Furthermore, there is the integral of p_j perturbation in the linearization process of f_j, thus we introduce additional variables to express the integral of p_j perturbation for simplifying the linearization of f_j.

Let $\zeta_j = \int \Delta p_j dt$, then $\frac{d\zeta_j}{dt} = \Delta p_j$. Let $\xi_j = \int \zeta_j dt$, then $\frac{d\xi_j}{dt} = \zeta_j$. The perturbation of f_j, i.e., Δf_j, can be expressed as

$$\begin{aligned}\Delta f_j = &-m_j \Delta P_{B\_j} + \frac{m_j k_{mP}}{N}\sum_{l\neq j}\frac{\zeta_l}{E_l} \\ &-\frac{(N-1)m_j k_{mP}}{N}\cdot\frac{\zeta_j}{E_j} + \frac{m_j k_{sj} k_{mI}}{N}\sum_{l\neq j}\frac{\xi_l}{E_l} \\ &-\frac{(N-1)m_j k_{sj} k_{mI}}{N}\cdot\frac{\xi_j}{E_j}\end{aligned} \tag{13}$$

Linearizing (11), (12), ζ_j and ε_j, the small-signal power controller model can be obtained as (14), in which including the outputs of the power controller, i.e., $[\Delta f_j, \Delta u_{odqj}^{*}]^T$.

$$\begin{aligned}
\begin{bmatrix}\Delta\dot{\theta}_j\\ \Delta\dot{P}_j\\ \Delta\dot{Q}_j\\ \dot{\zeta}_j\\ \dot{\xi}_j\end{bmatrix} &= A_{Pjj}\begin{bmatrix}\Delta\theta_j\\ \Delta P_j\\ \Delta Q_j\\ \zeta_j\\ \xi_j\end{bmatrix} + \sum_{l\neq j} A_{Pjl}\begin{bmatrix}\Delta\theta_l\\ \Delta P_l\\ \Delta Q_l\\ \zeta_l\\ \xi_l\end{bmatrix} \\
&\quad + B_{Pjj}\begin{bmatrix}\Delta i_{idqj}\\ \Delta u_{odqj}\\ \Delta i_{odqj}\end{bmatrix} + B_{fcom}[\Delta f_{com}] \\
\begin{bmatrix}\Delta f_j\\ \Delta u_{odqj}^{*}\end{bmatrix} &= \begin{bmatrix}A_{fjj}\\ A_{Ujj}\end{bmatrix}\begin{bmatrix}\Delta\theta_j\\ \Delta P_j\\ \Delta Q_j\\ \zeta_j\\ \xi_j\end{bmatrix} + \sum_{l\neq j}\begin{bmatrix}A_{fjl}\\ 0\end{bmatrix}\begin{bmatrix}\Delta\theta_l\\ \Delta P_l\\ \Delta Q_l\\ \zeta_l\\ \xi_l\end{bmatrix} \\
A_{Ujj} &= \begin{bmatrix}0 & 0 & -n_j & 0 & 0\\ 0 & 0 & 0 & 0 & 0\end{bmatrix},
\end{aligned} \tag{14}$$

where

$$A_{Pjj} = \begin{bmatrix} 0 & 0 & 0 & 0 & 0\\ -2\pi m_j & -\omega_c & 0 & 0 & 0\\ 0 & 0 & -\omega_c & 0 & 0\\ \frac{-2\pi(N-1)m_j k_{mP}}{NE_j} & 0 & 0 & 0 & 1\\ \frac{-2\pi(N-1)m_j k_{sj} k_{mI}}{NE_j} & 0 & 0 & 0 & 0\end{bmatrix}^T,$$

$$A_{Pjl} = \begin{bmatrix} 0 & 0 & 0 & \frac{2\pi m_j k_{mP}}{NE_l} & \frac{2\pi m_j k_{sj} k_{mI}}{NE_l}\\ 0 & 0 & 0 & 0 & 0\\ 0 & 0 & 0 & 0 & 0\\ 0 & 0 & 0 & 0 & 0\\ 0 & 0 & 0 & 0 & 0\end{bmatrix},$$

$$B_{Pjj} = \begin{bmatrix} 0 & 0 & 0 & 0 & 0\\ 0 & 0 & 0 & 0 & 0\\ 0 & \omega_c I_{odj} & \omega_c I_{oqj} & I_{odj} & 0\\ 0 & \omega_c I_{oqj} & -\omega_c I_{odj} & I_{oqj} & 0\\ 0 & \omega_c U_{odj} & -\omega_c U_{oqj} & U_{odj} & 0\\ 0 & \omega_c U_{oqj} & \omega_c U_{odj} & U_{oqj} & 0\end{bmatrix}^T$$

$$A_{fjj} = \begin{bmatrix} 0\\ -m_j\\ 0\\ \frac{-(N-1)m_j k_{mP}}{NE_j}\\ \frac{-(N-1)m_j k_{sj} k_{mI}}{NE_j}\end{bmatrix}^T, A_{fjl} = \begin{bmatrix} 0\\ 0\\ 0\\ \frac{m_j k_{mP}}{NE_l}\\ \frac{m_j k_{sj} k_{mI}}{NE_l}\end{bmatrix}^T,$$

$$B_{fcom} = \begin{bmatrix} -2\pi & 0 & 0 & 0 & 0\end{bmatrix}^T.$$

The voltage control loop in voltage & current dual-loop includes PI regulators to compare u_{odqj} with u_{odqj}^{*}, and feed-forward terms to compensate for output current disturbances [26]. The outputs of voltage control loop are i_{idqj}^{*}, which are used as the reference inputs of current control loop in voltage & current dual-loop. The current control loop also has PI regulators to compare i_{idqj}^{*} and i_{idqj}, and finally generate the PWM signal, i.e., u_{idqj}^{*}, which is shown in Fig. 2. The u_{idqj}^{*} is basically the output voltages of the converter, i.e., $u_{idqj}^{*} = u_{idqj}$. Thus we have

$$\begin{aligned}&\dot{\varphi}_{dj} = u_{odj}^{*} - u_{odj}, \quad \dot{\varphi}_{qj} = u_{oqj}^{*} - u_{oqj}\\ &\begin{cases} i_{idj}^{*} = k_{vP}(u_{odj}^{*} - u_{odj}) + k_{vI}\varphi_{dj} - \omega_n C_f u_{oqj} \\ \qquad + G i_{odj} \\ i_{iqj}^{*} = k_{vP}(u_{oqj}^{*} - u_{oqj}) + k_{vI}\varphi_{qj} + \omega_n C_f u_{odj} \\ \qquad + G i_{oqj}\end{cases}\end{aligned} \tag{15}$$

$$\begin{aligned}&\dot{\gamma}_{dj} = i_{idj}^{*} - i_{idj}, \quad \dot{\gamma}_{qj} = i_{iqj}^{*} - i_{iqj}\\ &\begin{cases} u_{idj}^{*} = k_{iP}(i_{idj}^{*} - i_{idj}) + k_{iI}\gamma_{dj} - \omega_n L_f i_{iqj} \\ u_{iqj}^{*} = k_{iP}(i_{iqj}^{*} - i_{iqj}) + k_{iI}\gamma_{qj} + \omega_n L_f i_{idj}\end{cases}\end{aligned} \tag{16}$$

where k_{vP} and k_{vI} are the proportional and integral coefficients of the PI regulators in voltage control loop. k_{iP} and k_{iI} are the proportional and integral coefficients of the PI regulators in current control loop. ω_n is the rated angular frequency, $\omega_n = 2\pi f_n$. G is feed-forward control gain. L_f and C_f are the inductance and capacitance of LC filter. φ_{dj} and φ_{qj} are the defined voltage difference state variables, and γ_{dj} and γ_{qj} are the defined current difference state variables in the voltage & current dual-loop.

Linearizing (15), (16) to be

$$\begin{bmatrix}\Delta\dot{\varphi}_{dj}\\ \Delta\dot{\varphi}_{qj}\end{bmatrix} = [0]\begin{bmatrix}\Delta\varphi_{dj}\\ \Delta\varphi_{qj}\end{bmatrix} + B_{u1}\begin{bmatrix}\Delta u^*_{odj}\\ \Delta u^*_{oqj}\end{bmatrix} + B_{u2}\begin{bmatrix}\Delta i_{idqj}\\ \Delta u_{odqj}\\ \Delta i_{odqj}\end{bmatrix}$$

$$\begin{bmatrix}\Delta i^*_{idj}\\ \Delta i^*_{iqj}\end{bmatrix} = C_u\begin{bmatrix}\Delta\varphi_{dj}\\ \Delta\varphi_{qj}\end{bmatrix} + D_{u1}\begin{bmatrix}\Delta u^*_{odj}\\ \Delta u^*_{oqj}\end{bmatrix} + D_{u2}\begin{bmatrix}\Delta i_{idqj}\\ \Delta u_{odqj}\\ \Delta i_{odqj}\end{bmatrix} \quad (17)$$

where

$$B_{u1} = \begin{bmatrix}1 & 0\\ 0 & 1\end{bmatrix},\quad B_{u2} = \begin{bmatrix}0 & 0 & -1 & 0 & 0 & 0\\ 0 & 0 & 0 & -1 & 0 & 0\end{bmatrix},$$
$$C_u = \begin{bmatrix}k_{vI} & 0\\ 0 & k_{vI}\end{bmatrix},\quad D_{u1} = \begin{bmatrix}k_{vP} & 0\\ 0 & k_{vP}\end{bmatrix},$$
$$D_{u2} = \begin{bmatrix}0 & 0 & -k_{vP} & -\omega_n C_f & G & 0\\ 0 & 0 & \omega_n C_f & -k_{vP} & 0 & G\end{bmatrix}.$$

$$\begin{bmatrix}\Delta\dot{\gamma}_{dj}\\ \Delta\dot{\gamma}_{qj}\end{bmatrix} = [0]\begin{bmatrix}\Delta\gamma_{idj}\\ \Delta\gamma_{iqj}\end{bmatrix} + B_{i1}\begin{bmatrix}\Delta i^*_{idj}\\ \Delta i^*_{iqj}\end{bmatrix} + B_{i2}\begin{bmatrix}\Delta i_{idqj}\\ \Delta u_{odqj}\\ \Delta i_{odqj}\end{bmatrix}$$

$$\begin{bmatrix}\Delta u^*_{idj}\\ \Delta u^*_{iqj}\end{bmatrix} = C_i\begin{bmatrix}\Delta\gamma_{idj}\\ \Delta\gamma_{iqj}\end{bmatrix} + D_{i1}\begin{bmatrix}\Delta i^*_{idj}\\ \Delta i^*_{iqj}\end{bmatrix} + D_{i2}\begin{bmatrix}\Delta i_{idqj}\\ \Delta u_{odqj}\\ \Delta i_{odqj}\end{bmatrix} \quad (18)$$

where

$$B_{i1} = \begin{bmatrix}1 & 0\\ 0 & 1\end{bmatrix},\quad B_{i2} = \begin{bmatrix}-1 & 0 & 0 & 0 & 0 & 0\\ 0 & -1 & 0 & 0 & 0 & 0\end{bmatrix},$$
$$C_i = \begin{bmatrix}k_{iI} & 0\\ 0 & k_{iI}\end{bmatrix},\quad D_{i1} = \begin{bmatrix}k_{iP} & 0\\ 0 & k_{iP}\end{bmatrix},$$
$$D_{i2} = \begin{bmatrix}-k_{iP} & -\omega_n L_f & 0 & 0 & 0 & 0\\ \omega_n L_f & -k_{iP} & 0 & 0 & 0 & 0\end{bmatrix}.$$

The equations about LC filter and coupling inductor are

$$\begin{cases}\dot{i}_{idj} = \dfrac{-R_f}{L_f}i_{idj} + \omega i_{iqj} + \dfrac{1}{L_f}u_{idj} - \dfrac{1}{L_f}u_{odj}\\ \dot{i}_{iqj} = \dfrac{-R_f}{L_f}i_{iqj} - \omega i_{idj} + \dfrac{1}{L_f}u_{iqj} - \dfrac{1}{L_f}u_{oqj}\\ \dot{u}_{odj} = \dfrac{1}{C_f}i_{idj} - \dfrac{1}{C_f}i_{odj} + \omega u_{oqj}\\ \dot{u}_{oqj} = \dfrac{1}{C_f}i_{iqj} - \dfrac{1}{C_f}i_{oqj} - \omega u_{odj}\\ \dot{i}_{odj} = \dfrac{-R_c}{L_c}i_{odj} + \omega i_{oqj} + \dfrac{1}{L_c}u_{odj} - \dfrac{1}{L_c}u_{bdj}\\ \dot{i}_{oqj} = \dfrac{-R_c}{L_c}i_{oqj} - \omega i_{odj} + \dfrac{1}{L_c}u_{oqj} - \dfrac{1}{L_c}u_{bqj}\end{cases} \quad (19)$$

where R_f is the resistance of LC filter. L_c and R_c are the inductance and resistance of coupling inductor. ω is angular frequency, $\omega = 2\pi f$. u_{bdj} and u_{bqj} are the voltages at the connection point between the jth BESS unit and the AC bus. Let $\omega_0 = 2\pi f_0$ denotes the system steady-state angular frequency, and then (19) is linearized to be

$$\begin{bmatrix}\Delta\dot{i}_{idqj}\\ \Delta\dot{u}_{odqj}\\ \Delta\dot{i}_{odqj}\end{bmatrix} = A_o\begin{bmatrix}\Delta i_{idqj}\\ \Delta u_{odqj}\\ \Delta i_{odqj}\end{bmatrix} + B_{o1}\begin{bmatrix}\Delta u^*_{idj}\\ \Delta u^*_{iqj}\end{bmatrix} + B_{o2}\begin{bmatrix}\Delta u_{bdj}\\ \Delta u_{bqj}\end{bmatrix} + B_{ofj}\left[\Delta f_j\right] \quad (20)$$

where

$$A_o = \begin{bmatrix}\frac{-R_f}{L_f} & \omega_0 & \frac{-1}{L_f} & 0 & 0 & 0\\ -\omega_0 & \frac{-R_f}{L_f} & 0 & \frac{-1}{L_f} & 0 & 0\\ \frac{1}{C_f} & 0 & 0 & \omega_0 & \frac{-1}{C_f} & 0\\ 0 & \frac{1}{C_f} & -\omega_0 & 0 & 0 & \frac{-1}{C_f}\\ 0 & 0 & \frac{1}{L_c} & 0 & \frac{-R_c}{L_c} & \omega_0\\ 0 & 0 & 0 & \frac{1}{L_c} & -\omega_0 & \frac{-R_c}{L_c}\end{bmatrix},$$

$$B_{o1} = \begin{bmatrix}\frac{1}{L_f} & 0\\ 0 & \frac{1}{L_f}\\ 0 & 0\\ 0 & 0\\ 0 & 0\\ 0 & 0\end{bmatrix},\quad B_{o2} = \begin{bmatrix}0 & 0\\ 0 & 0\\ 0 & 0\\ 0 & 0\\ \frac{-1}{L_c} & 0\\ 0 & \frac{-1}{L_c}\end{bmatrix},$$

$$B_{ofj} = 2\pi\begin{bmatrix}I_{iqj} & -I_{idj} & U_{oqj} & -U_{odj} & I_{oqj} & -I_{odj}\end{bmatrix}^T.$$

The u_{bdj} and u_{bqj} should be translated to the common frame to connect the jth converter to the whole system model [27]. Thus $[\Delta u_{bdj}, \Delta u_{bqj}]^T$ in (20) are expressed as

$$\begin{bmatrix}\Delta u_{bdj}\\ \Delta u_{bqj}\end{bmatrix} = A_{bj}\begin{bmatrix}\Delta u_{bD}\\ \Delta u_{bQ}\end{bmatrix} + B_{\theta j}\begin{bmatrix}\Delta\theta_j\\ \Delta P_j\\ \Delta Q_j\\ \zeta_j\\ \xi_j\end{bmatrix} \quad (21)$$

where u_{bD} and u_{bQ} are the voltages at the connection point between the first BESS unit that is taken as common frame and AC bus, i.e., u_{bD} and u_{bQ} are actually the u_{bd1} and u_{bq1},

$$A_{bj} = \begin{bmatrix}\cos\theta_{0j} & \sin\theta_{0j}\\ -\sin\theta_{0j} & \cos\theta_{0j}\end{bmatrix},$$
$$B_{\theta j} = \begin{bmatrix}-U_{bD}\sin\theta_{0j} + U_{bQ}\cos\theta_{0j} & 0 & 0 & 0 & 0\\ -U_{bD}\cos\theta_{0j} - U_{bQ}\sin\theta_{0j} & 0 & 0 & 0 & 0\end{bmatrix}.$$

Combining with (14), (17), (18), (20) and (21), the small-signal model of the jth BESS unit is obtained as

$$\left[\Delta\dot{x}_j\right] = A_{jj}\left[\Delta x_j\right] + B_{jj}[\Delta u_{bDQ}] + B_{jcom}[\Delta f_{com}] + \sum_{l\neq j} A_{jl}[\Delta x_l]$$

$$\text{where } [\Delta f_{com}] = F_{f1}[\Delta x_1] + \sum_{l \neq 1} F_{fl}[\Delta x_l] \tag{22}$$

where $\Delta x_j = [\Delta\theta_j, \Delta P_j, \Delta Q_j, \zeta_j, \varepsilon_j, \Delta\varphi_{dqj}, \Delta\gamma_{dqj}, \Delta i_{idqj}, \Delta u_{odqj}, \Delta i_{odqj}]^T$, $\Delta x_l = [\Delta\theta_l, \Delta P_l, \Delta Q_l, \zeta_l, \varepsilon_l, \Delta\varphi_{dql}, \Delta\gamma_{dql}, \Delta i_{idql}, \Delta u_{odql}, \Delta i_{odql}]^T$. Δx_j is a state vector for jth BESS unit including 15 varibles, and Δx_l is a state vector for lth BESS unit including 15 varibles. $[\Delta u_{bDQ}] = [\Delta u_{bD}, \Delta u_{bQ}]^T$,

$$B_{jj} = \begin{bmatrix} 0 \\ 0 \\ 0 \\ B_{o2}A_{bj} \end{bmatrix}_{15\times 2}, \quad B_{jcom} = \begin{bmatrix} B_{fcom} \\ 0 \\ 0 \\ 0 \end{bmatrix}_{15\times 1},$$

$$F_{f1} = \begin{bmatrix} A_{f11} \\ 0 \\ 0 \\ 0 \end{bmatrix}^T_{15\times 1},$$

$$A_{jl} = \begin{bmatrix} A_{Pjl} & 0 & 0 & 0 \\ 0 & 0 & 0 & 0 \\ 0 & 0 & 0 & 0 \\ B_{ofj}A_{fjl} & 0 & 0 & 0 \end{bmatrix}_{15\times 15}, \quad F_{f1} = \begin{bmatrix} A_{f11} \\ 0 \\ 0 \\ 0 \end{bmatrix}^T_{15\times 1},$$

$$F_{fl} = \begin{bmatrix} A_{f1l} & 0 & 0 & 0 \end{bmatrix}_{1\times 15},$$

$$A_{jj} = \begin{bmatrix} A_{Pjj} & 0 & 0 & B_{Pjj} \\ B_{u1}A_{Ujj} & 0 & 0 & B_{u2} \\ B_{i1}D_{u1}A_{Ujj} & B_{i1}C_u & 0 & B_{i2}+B_{i1}D_{u2} \\ B_{o1}D_{i1}D_{u1}A_{Ujj} + B_{o2}B_{\theta j} + B_{ofj}A_{fjj} & B_{o1}D_{i1}C_u & B_{o1}C_i & A_O + B_{o1}D_{i2} + B_{o1}D_{i1}D_{u2} \end{bmatrix}_{15\times 15}.$$

For N BESS units operated in parallel in microgrid, a complete small-signal state space model including $15\times N$ state varibles is as follows

$$[\dot{\Delta x}] = A_M[\Delta x] + B_M[\Delta u_{bDQ}] \tag{23}$$

where $[\Delta x] = [\Delta x_1, \Delta x_2, \ldots, \Delta x_N]^T$,

$$A_M = \begin{bmatrix} A_{11} & A_{21} + B_{2com}F_{f1} & \ldots & A_{N1} + B_{Ncom}F_{f1} \\ A_{12} & A_{22} + B_{2com}F_{f2} & \ldots & A_{N2} + B_{Ncom}F_{f2} \\ \ldots & \ldots & \ldots & \ldots \\ A_{1N} & A_{2N} + B_{2com}F_{fN} & \ldots & A_{NN} + B_{Ncom}F_{fN} \end{bmatrix}^T_{15N\times 15N},$$

$$B_M = \begin{bmatrix} B_{11} & B_{22} & \ldots & B_{NN} \end{bmatrix}^T_{2\times 15N}.$$

Since the SoC balance is the subject in this paper, the control parameters of the proposed improved *P-f* droop method are mainly investigated based on the state matrix of the model described in (23), i.e., A_M. A microgrid consisting of four BESS units is shown in Fig. 3, and the relevant structure and control parameters are shown in Table 1, in which $n_1 = n_2 = n_3 = n_4$. In order to obtain the appropriate values of k_{mP} and k_{mI}, k_{sj}, $j = 1, 2, 3, 4$, should be set to be one in the small signal analysis. A_M and the relevant structure and control parameters are used to calculate the root locus of low-frequency eigenvalues with the variations of k_{mP} and k_{mI}. The root locus of dominant eigenvalues are shown as Fig. 4(a) and Fig. 4(b), in which k_{mP} increasing from 0.1 to 30 in Fig. 4(a), and k_{mI} increasing from 0.0001 to 0.075 in Fig. 4(b).

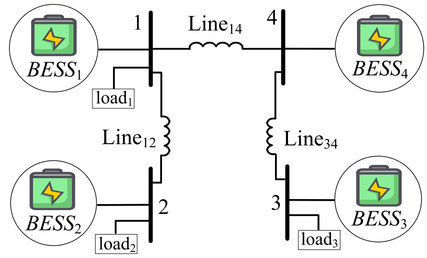

FIGURE 3. System of BESSs for small signal analysis.

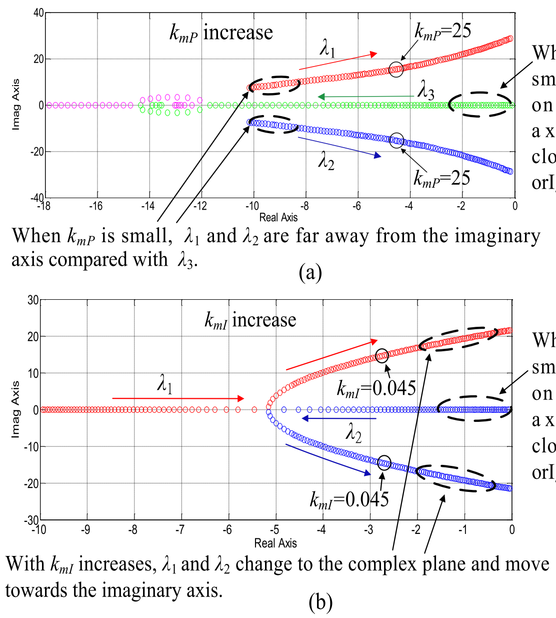

FIGURE 4. Eigenvalue analysis of the SoC based droop (a) Eigenvalue trace with k_{mP} increasing, (b) Eigenvalue trace with k_{mI} increasing.

Fig. 4(a) shows that the eigenvalues marked with λ_3 are on the real axis and close to the origin when k_{mP} is small. Compared with λ_1 and λ_2, which are far away from the imaginary axis, λ_3 is the most dominant and crucial for system stability. However, the system is in an overdamped state since λ_3 is on the real axis. With k_{mP} increases, λ_3 moves away from the imaginary axis, but λ_1 and λ_2 move towards it. When λ_1 and λ_2 are closer to the imaginary axis than λ_3, λ_1 and λ_2 become the dominant eigenvalues. Then the system is in an underdamped state since λ_1 and λ_2 are on the complex plane. The damping ratio of the system will be decreased with λ_1 or λ_2 gradually approaches the imaginary axis, which causes a more oscillating transient process. It should be noted that the transient process is slow before the system reaches stability when its damping is large, that is system is in an overdamped state, while the transient process will be more and more oscillatory when the damping ratio of system is decreased [27]. Although the system is ultimately stable for k_{mP} increasing from 0.1 to 30 since all the low-frequency eigenvalues are in the left half-plane as shown in Fig. 4(a), what we expect is that the system has neither too much damping nor a more oscillating transient process. Thus the low-frequency dominant eigenvalue can neither be on the real axis nor very close to the imaginary axis. The k_{mP} is set to be 25 based on the above analysis. The selection of k_{mI} is very similar to that of k_{mP}, so we will not go into details here. The k_{mI} is set to be 0.045 in this paper since the corresponding low-frequency dominant eigenvalues are in complex plane and they are not very close to the imaginary axis as shown in Fig. 4(b), which ensures that the transient process of system is neither too slow nor too oscillatory.

B. PARAMETERS DESIGN OF DYNAMIC AVERAGE CONSENSUS ALGORITHM

The average SoC is calculated by the agent of each BESS unit using (10). It is desired that the average SoC can be obtained stably and rapidly. Actually, the dynamic average consensus algorithm can converge the SoC discovered by each agent to a common value as long as the studied topology is connected which has been proved in [20], [25]. In order to select the appropriate value of α for obtaining the average SoC in each agent, we tested the four BESS units as shown in Fig. 3, which has four agents. Assuming the initial values of the four state variables, i.e., $x(j)$, $j = 1, 2, 3, 4$, are 30, 40, 50 and 60, respectively. The convergent results with different values of α are shown in Fig. 5.

Fig. 5(a) and 5(b) show that the four state variables can converge to a common value with $\alpha = 0.1$ and $\alpha = 0.25$, but the convergent speed with $\alpha = 0.1$ is slower than that with $\alpha = 0.25$. The four state variables have some fluctuations in the process of convergence with $\alpha = 0.4$, and they cannot converge when α is 0.5. The consensus algorithm will be divergent if α is greater than 0.5 as shown in Fig. 5(e). It can be seen that the consensus algorithm converges very slowly when α is very small, but the algorithm will diverge when α is very large.

IV. SIMULATION VERIFICATION

The MATLAB/simulink model of the microgrid shown in Fig. 6 is built to verify the proposed SoC-based droop control for balancing SoC. The AC microgrid running in autonomous mode consists of four paralleled BESS units and their agents, a PV generation unit, a WT generation unit and several loads. The α in (12) is set to be 0.25. The PV and WT units are used as RESs and operated in MPPT mode. Assuming that the total active power output of PV and WT is 30kW, and the RESs output is not shown in the simulation diagram since it is not the focus of the paper. The initial values of SoC_1, SoC_2, SoC_3 and SoC_4 are 70%, 60%, 80% and 90% as shown in Fig. 6. The BESS uses droop control to supply frequency and voltage support to the system.

TABLE 1. System structure and control parameters.

Item	Symbol	Value
LC Filter	L_f/	2.3mH/
inductance/capacitor	C_f/	11.02μF/
/resistance	R_f	0.01Ω
Coupling inductor	L_c/R_c	1mH/0.2Ω
inductance/ resistance		
Line impedance of line_{12}	L_{12}/R_{12}	0.2mH/0.4Ω
Line impedance of line_{14}	L_{14}/R_{14}	0.23mH/0.5Ω
Line impedance of line_{34}	L_{34}/R_{34}	0.3mH/0.6Ω
Nominal frequency/voltage	f_n/ V_n	50Hz/311V
Upper and lower limits of	f_{max}/	50.5Hz/
frequency variation range	f_{min}	49.5Hz
Cut-off frequency	ω_c	30rad/s
Threshold of SoC	d_{SoC}	0.01%
Capacities of BESS	E_1/	25000(Ah·V)$^{-1}$/
units 1/2/3/4	E_2/	37500(Ah·V)$^{-1}$/
	E_3/	37500(Ah·V)$^{-1}$/
	E_4	50000(Ah·V)$^{-1}$
Frequency droop coefficients	m_1/	0.05Hz/kW/
	m_2/	0.0333Hz/kW/
	m_3/	0.0333Hz/kW/
	m_4	0.025Hz/kW
Voltage droop coefficients	$n_1/n_2/n_3/n_4$	1.5V/kVar
Resistance of RL loads	R_{load1}/R_{load2}/	14.4Ω/14.4Ω/
	R_{load3}	14.4Ω
Inductance of RL loads	L_{load1}/L_{load2}/	0.23H/0.23H/
	L_{load3}	0.23H
Voltage control of dual loop	k_{vP}, k_{vI}	2, 8s^{-1}
Current control of dual loop	kiP, kiI	10, 200s^{-1}

The impedance values of load_1, load_2 and load_3 are given in Table 1. $\text{Load}_4 = R_{load4}+jX_{load4}$, in which $R_{load4} = 3.6\Omega$ and $X_{load4} = 2\pi f L_{load4}$, $L_{load4} = 0.23$H. The capacity ratio of the four batteries is 1:1.5:1.5:2, thus m_1: m_2: m_3: $m_4 = 6 : 4 : 4 : 3$ as shown in Table 1. The capacity of BESS unit 2 is equal to that of BESS unit 3, which is used to verify the proposed strategy can balance SoC when different batteries have the same capacity. While the capacity of BESS unit 2 is different from that of BESS unit 1, or that of BESS unit 4, which is used to verify the proposed strategy can balance SoC in the case that different batteries have different capacities. Since voltage and reactive power are not the focus of this paper, they are not analyzed in simulation.

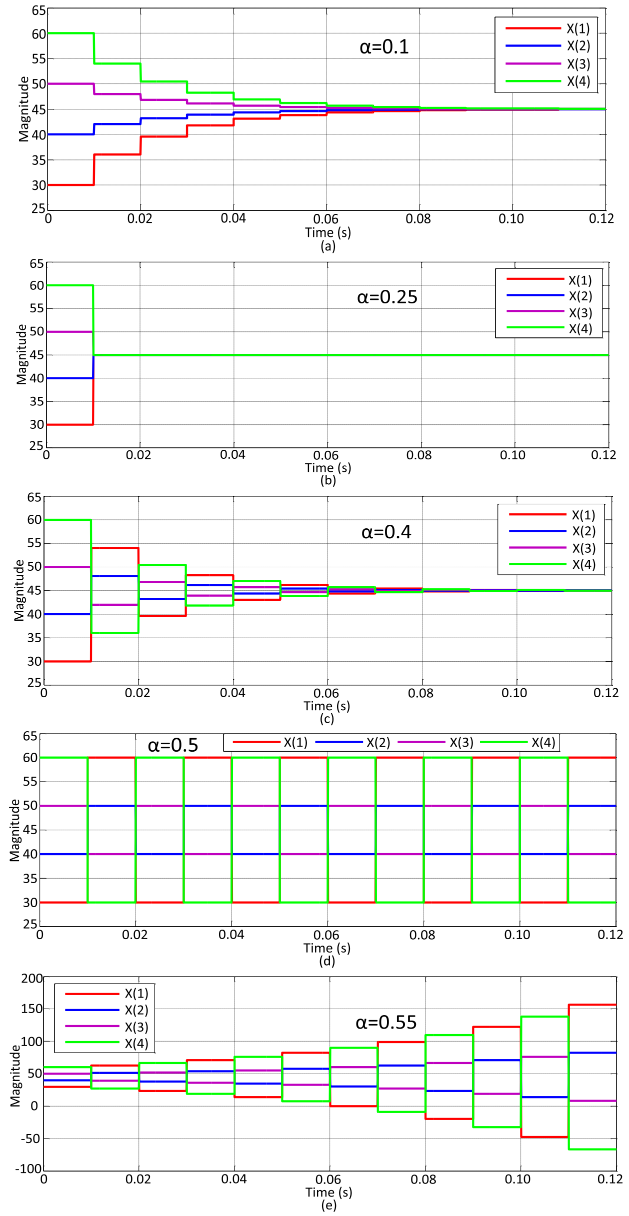

FIGURE 5. Convergence results (a) $\alpha = 0.1$, (b) $\alpha = 0.25$, (c) $\alpha = 0.4$, (d) $\alpha = 0.5$, (e) $\alpha = 0.55$.

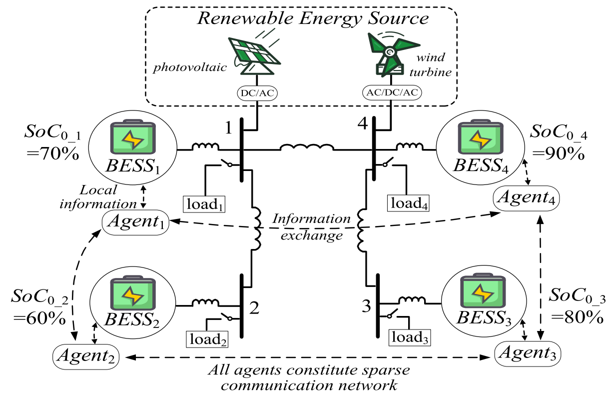

FIGURE 6. An AC microgrid with BESSs and RESs.

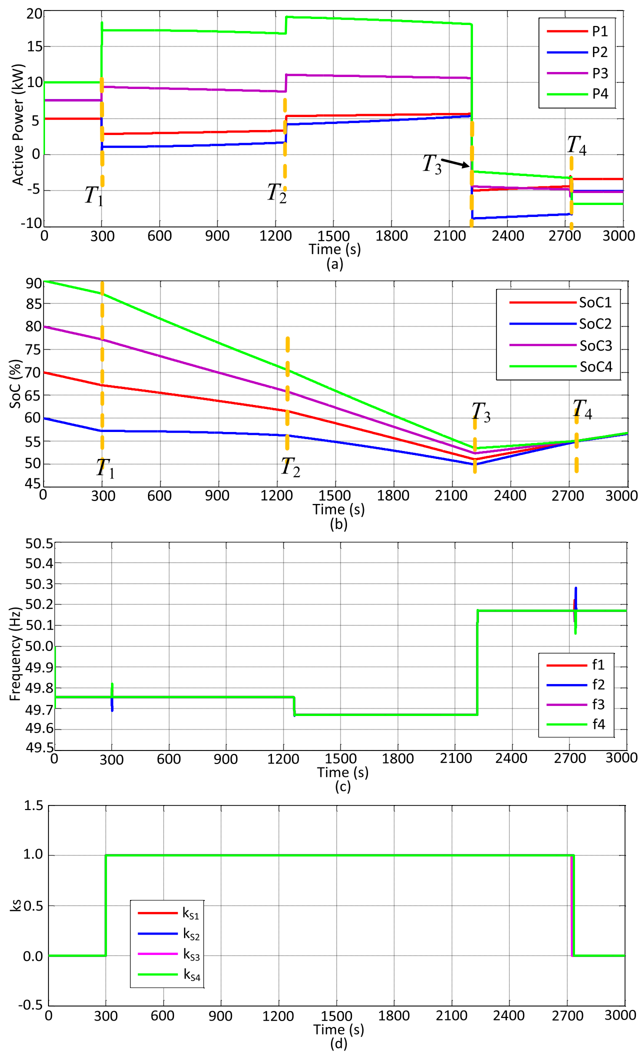

FIGURE 7. Simulation results in SoC balance verification: (a) Active power; (b) SoC; (c) Frequency; (d) Judgment signal.

A. SoC BALANCE VERIFICATION

In this case study, the simulation is divided into 4 stages for verifying the effectiveness of the proposed strategy. The simulation results are shown in Fig. 7. Fig. 7(a), Fig. 7(b), Fig. 7(c) and Fig. 7(d) shows the active power outputs, SoCs, output frequencies and the judgment signals, i.e., k_{sj}, $j = 1,2,3,4$, of the four BESS units, respectively.

Stage 1 ($0 \sim T_1$): Load$_1$, load$_2$ and load$_4$ are connected to the system during this stage. The conventional P-f droop, i.e., (1), is used for BESS. Fig. 7(a) shows that all active powers are positive, which illustrates that the RESs output cannot meet the load consumption. $P_1 = 5$kW, $P_2 = P_3 = 7.5$kW and $P_4 = 10$kW at stage 1, and SoC_1, SoC_2, SoC_3 and SoC_4 decrease at the same rate as shown in Fig. 7(b), which shows that once the droop coefficients of P-f are set to be inversely proportional to their capacities, the rate of change of SoC will be equal. Since the SoC-based droop is not activated, $k_{sj} = 0$, $j = 1, 2, 3, 4$.

Stage 2 ($T_1 \sim T_2$): The SoC-based droop is activated at the time of T_1. Since the difference between SoC_j, $j = 1, 2, 3, 4$, and SoC_{ave} is larger than d_{SoC}, Fig. 7(d) shows that $k_{sj} = 1$ in this stage. Fig. 7(a) shows that the active power of each BESS unit changes to a new value under the regulation of PI item in (7) at the time of T_1, which causes all SoCs starting to converge. The PI item varies with the variation of (SoC_j-SoC_{ave}), which results in the variation of P_j, but all SoCs always change towards consistency during stage 2 as shown in Fig. 7(b).

Stage 3 ($T_2 \sim T_3$): Load$_3$ is connected at the time of T_2 to investigate the impact of step load changes on the proposed strategy. After load$_3$ is connected, all BESS units increase their active power outputs, but all SoCs continue converging, which illustrates that there is no effect on SoC balance of the load variation.

Stage 4 (after T_3): Load$_2$, load$_3$ and load$_4$ are cut out at the time of T_3, and then all active powers become negative values as shown in Fig. 7(a), which illustrates that all BESS units start to absorb the excess power of RESs. Fig. 7(b) shows that all SoCs continue to change towards consistency during stage 4, which illustrates that the proposed strategy can make different SoCs change towards consistency by using a unified control method in both charging and discharging state. Finally, SoC balance is achieved at the time of T_4. Fig. 7(d) shows that k_{sj} becomes zero, and then the PI item in (7) is almost zero for each BESS unit. After that, all BESS units absorb the power according to the inversely ratio of the *P-f* droop coefficients and all SoCs vary at the same rate.

Fig. 7(c) shows that the output frequencies of all BESS units are always kept in a safe range, i.e., [49.5Hz, 50.5Hz], during the whole process. It should be noted that the out power of some unit may be limited by PI in some case, but other units can output or absorb more power through the regulation of the proposed strategy since it is a coordinated control strategy for all BESS units to reasonably distribute the total power shortage or surplus power.

B. THE FUNCTION OF INTEGRAL ITEM IN THE PROPOSED DROOP

The proposed SoC-based droop control, i.e., (7), can be expressed in another way, that is

$$\begin{aligned} f_j &= [f_n + m_j k_{mP}(SoC_j - SoC_{ave}) \\ &\quad + m_j k_{sj} k_{mI} \int (SoC_j - SoC_{ave}) dt] - m_j P_{B\_j} \\ where\ k_{sj} &= \begin{cases} 1, & if\, |SoC_j - SoC_{ave}| \geq d_{SoC} \\ 0, & if\, |SoC_j - SoC_{ave}| < d_{SoC} \end{cases} \end{aligned} \tag{24}$$

Equation (24) shows that the proposed droop is actually a frequency scheduling method by adding a proportional item and an integral item into the nominal frequency. A similar frequency scheduling approach has been proposed in [20], in which the adjustment item is a proportional item. In order

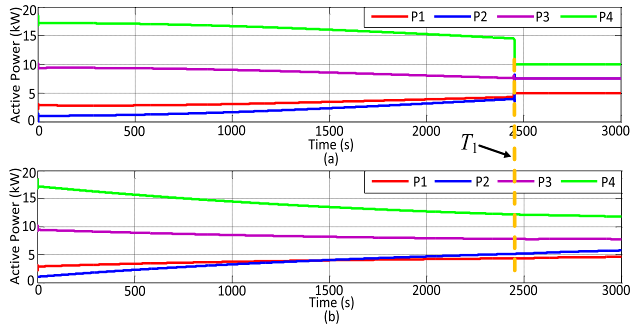

FIGURE 8. The active powers of the four BESS units: (a) the method with PI item; (b) the method with only P item.

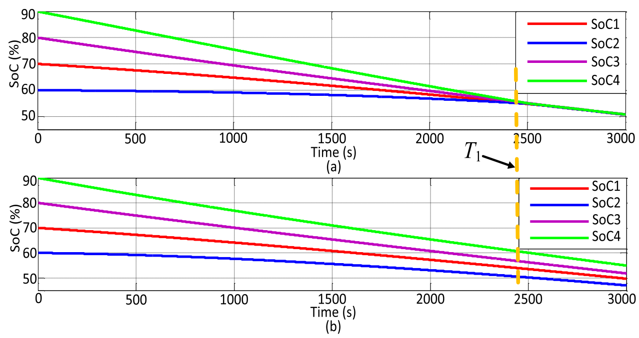

FIGURE 9. The SoCs of the four BESS units: (a) the method with PI item; (b) the method with only P item.

to investigate the function of the integral item in the proposed method of this paper for demonstrating the advantages, a comparative case is studied by comparing the method proposed in this paper, i.e., (7), with the frequency scheduling approach containing only proportional item as proposed in [20]. Load$_1$, load$_2$ and load$_4$ are connected to the system and the RESs output cannot meet the load consumption, and then BESS is in discharging state. The active powers of the four BESS units under the regulation of the method proposed in this paper are shown in Fig. 8(a), and that under the regulation of the method containing only proportional item are shown in Fig. 8(b). The SoCs of the four BESS units under the regulation of the method proposed in this paper are shown in Fig. 9(a), and that under the regulation of the method containing only proportional item are shown in Fig. 9(b).

Fig. 8(a) and Fig. 8(b) show that the differences between different active powers under the regulation of (7) are larger than that between different active powers under the regulation of the method containing only proportional item before SoC reaches balance, e.g. the difference between P_2 and P_3 in Fig. 8(a) is larger than that between P_2 and P_3 in Fig. 8(b) at the time of 1500s, which shows that SoC_2 and SoC_3 will converge to a common value faster by using (7) than that by using the method in [20]. Fig. 9(a) and Fig. 9(b) intuitively show that the SoC balance is achieved at the time of T_1 by using the method proposed in this paper, but the SoC has not reached balance at T_1 by using the method containing

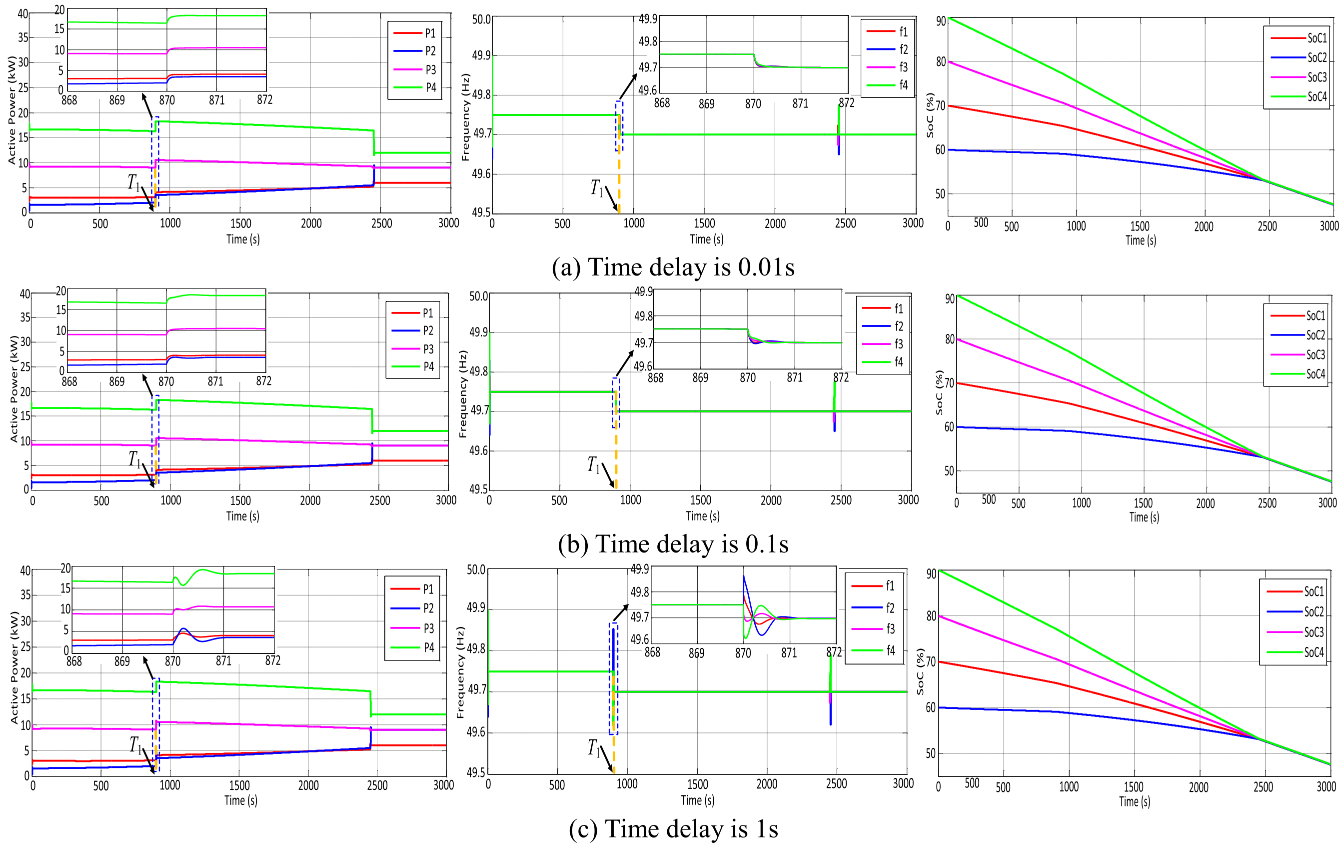

FIGURE 10. The dynamics of active power, frequency and SoC under different delay: (a) Time delay is 0.01s; (b) Time delay is 0.1s; (c) Time delay is 1s.

only proportional item. The simulation results in this case study demonstrate that the integral item in (7) can speed up SoC balance, and rapid SoC equalization can avoid overcharge or deep discharge in some of the storage unit more effectively and improve the effective utilization of BESS.

C. THE IMPACT OF COMMUNICATION DELAY

Since the proposed SoC-based droop relies on MAS to exchange information and there is usually time delay in actual sparse communication network, the impact of different time delay on the proposed method is investigated in this case study. Load_1, load_2 and load_4 are connected to the system at the beginning and load_3 is connected at the time of T_1. Fig. 10(a), Fig. 10(b) and Fig. 10(c) show the dynamics of active powers, frequencies and SoCs under the time delay of 0.01s, 0.1s and 1s, respectively. Fig. 10(a) shows that the active powers and output frequencies of the four BESS units vary smoothly to new state values after load changes at T_1, and the SoC continues changing towards consistency and finally achieves balance. Fig. 10(b) shows that the active powers and output frequencies have very small fluctuations after load_3 is connected, but the dynamic convergence characteristics of SoC are almost unaffected. Fig. 10(c) shows that the active powers and output frequencies fluctuate obviously after load changes. However, the dynamic convergence characteristics of SoC are almost unaffected just like the case in Fig. 10(b), which is due to the time constant of the SoC estimation based on integrator is generally large. The simulation results of this case study show that the proposed method can achieve SoC balance even if the communication network has a certain time delay and reasonable time delay has almost no effect on the dynamic convergence characteristics of SoC.

V. CONCLUSION

This paper focused on balancing SoC by regulating the charging and discharging power of BESS. The conclusions of this study are as follows:

1) An improved SoC-based droop control is proposed to achieve SoC balance for multiple BESS units by utilizing MAS. A proportional-integral adjustment item using average SoC is added to the nominal frequency for regulating the charging and discharging power of BESS, and the proposed method need not be changed in different operating mode compared with the adaptive droop gain methods. In addition, the function of integral item in improved droop control is investigated and simulation results show that it can speed up SoC balance.

2) In order to select the appropriate control parameters of the improved droop control, the small-signal state space model of BESS is built. The model includes the state variables

of all BESS units, thus the control parameters can be set reasonably through small signal analysis no matter how many BESS units are included in the system, which improves the applicability of the proposed method. Simulation results show that the proposed method can balance SoC effectively regardless of whether the capacities of different batteries are the same based on the setting control parameters.

3) The impact of a certain time delay on SoC balance is investigated. Simulation results show that even if there is a certain time delay in communication network, it has almost no effect on SoC balance by using the improved droop based on MAS, which improves the system reliability.

REFERENCES

[1] H. Al Haj Hassan, A. Pelov, and L. Nuaymi, "Integrating cellular networks, smart grid, and renewable energy: Analysis, architecture, and challenges," *IEEE Access*, vol. 3, pp. 2755–2770, 2015.

[2] J. Ahmed and Z. Salam, "A modified P&O maximum power point tracking method with reduced steady-state oscillation and improved tracking efficiency," *IEEE Trans. Sustain. Energy*, vol. 7, no. 4, pp. 1506–1515, Oct. 2016.

[3] Y. Xu, W. Zhang, G. Hug, S. Kar, and Z. Li, "Cooperative control of distributed energy storage systems in a microgrid," *IEEE Trans. Smart Grid*, vol. 6, no. 1, pp. 238–248, Jan. 2015.

[4] R. Tonkoski, L. A. C. Lopes, and T. H. M. El-Fouly, "Coordinated active power curtailment of grid connected PV inverters for overvoltage prevention," *IEEE Trans. Sustain. Energy*, vol. 2, no. 2, pp. 139–147, Apr. 2011.

[5] J.-T. Su and C.-W. Liu, "A novel phase-shedding control scheme for improved light load efficiency of multiphase interleaved DC–DC converters," *IEEE Trans. Power Electron.*, vol. 28, no. 10, pp. 4742–4752, Oct. 2013.

[6] C. A. Hill, M. C. Such, D. Chen, J. Gonzalez, and W. M. Grady, "Battery energy storage for enabling integration of distributed solar power generation," *IEEE Trans. Smart Grid*, vol. 3, no. 2, pp. 850–857, Jun. 2012.

[7] S. A. Abdelrazek and S. Kamalasadan, "Integrated PV capacity firming and energy time shift battery energy storage management using energy-oriented optimization," *IEEE Trans. Ind. Appl.*, vol. 52, no. 3, pp. 2607–2617, May 2016.

[8] D. Wu, F. Tang, T. Dragicevic, J. C. Vasquez, and J. M. Guerrero, "Autonomous active power control for islanded AC microgrids with photovoltaic generation and energy storage system," *IEEE Trans. Energy Convers.*, vol. 29, no. 4, pp. 882–892, Dec. 2014.

[9] C. Li, T. Dragicevic, N. L. Diaz, J. C. Vasquez, and J. M. Guerrero, "Voltage scheduling droop control for State-of-Charge balance of distributed energy storage in DC microgrids," in *Proc. IEEE Int. Energy Conf. (ENERGYCON)*, Cavtat Croatia, May 2014, pp. 1310–1314.

[10] T. Morstyn, A. V. Savkin, B. Hredzak, and V. G. Agelidis, "Multi-agent sliding mode control for state of charge balancing between battery energy storage systems distributed in a DC microgrid," *IEEE Trans. Smart Grid*, vol. 9, no. 5, pp. 4735–4743, Sep. 2018.

[11] N. L. Diaz, A. C. Luna, J. C. Vasquez, and J. M. Guerrero, "Centralized control architecture for coordination of distributed renewable generation and energy storage in islanded AC microgrids," *IEEE Trans. Power Electron.*, vol. 32, no. 7, pp. 5202–5213, Jul. 2017.

[12] M. Karimi, P. Wall, H. Mokhlis, and V. Terzija, "A new centralized adaptive underfrequency load shedding controller for microgrids based on a distribution state estimator," *IEEE Trans. Power Del.*, vol. 32, no. 1, pp. 370–380, Feb. 2017.

[13] H. K. Morales-Paredes, J. P. Bonaldo, and J. A. Pomilio, "Centralized control center implementation for synergistic operation of distributed multifunctional single-phase grid-tie inverters in a microgrid," *IEEE Trans. Ind. Electron.*, vol. 65, no. 10, pp. 8018–8029, Oct. 2018.

[14] X. Lu, K. Sun, J. M. Guerrero, J. C. Vasquez, and L. Huang, "Double-quadrant State-of-Charge-Based droop control method for distributed energy storage systems in autonomous DC microgrids," *IEEE Trans. Smart Grid*, vol. 6, no. 1, pp. 147–157, Jan. 2015.

[15] X. Lu, K. Sun, J. M. Guerrero, J. C. Vasquez, and L. Huang, "State-of-Charge balance using adaptive droop control for distributed energy storage systems in DC microgrid applications," *IEEE Trans. Ind. Electron.*, vol. 61, no. 6, pp. 2804–2815, Jun. 2014.

[16] Y. Xia, M. Yu, P. Yang, Y. Peng, and W. Wei, "Generation-storage coordination for islanded DC microgrids dominated by PV generators," *IEEE Trans. Energy Convers.*, vol. 34, no. 1, pp. 130–138, Mar. 2019.

[17] T. Morstyn, B. Hredzak, G. D. Demetriades, and V. G. Agelidis, "Unified distributed control for DC microgrid operating modes," *IEEE Trans. Power Syst.*, vol. 31, no. 1, pp. 802–812, Jan. 2016.

[18] W. Huang and J. A. Abu Qahouq, "Energy sharing control scheme for State-of-Charge balancing of distributed battery energy storage system," *IEEE Trans. Ind. Electron.*, vol. 62, no. 5, pp. 2764–2776, May 2015.

[19] T. Morstyn, M. Momayyezan, B. Hredzak, and V. G. Agelidis, "Distributed control for State-of-Charge balancing between the modules of a reconfigurable battery energy storage system," *IEEE Trans. Power Electron.*, vol. 31, no. 11, pp. 7986–7995, Nov. 2016.

[20] C. Li, E. A. A. Coelho, T. Dragicevic, J. M. Guerrero, and J. C. Vasquez, "Multiagent-based distributed state of charge balancing control for distributed energy storage units in AC microgrids," *IEEE Trans. Ind. Appl.*, vol. 53, no. 3, pp. 2369–2381, May 2017.

[21] Q. Shafiee, J. M. Guerrero, and J. C. Vasquez, "Distributed secondary control for islanded Microgrids—A novel approach," *IEEE Trans. Power Electron.*, vol. 29, no. 2, pp. 1018–1031, Feb. 2014.

[22] Z. Yang, S. Yu, W. Lou, and C. Liu, "P^2: Privacy-preserving communication and precise reward architecture for V2G networks in smart grid," *IEEE Trans. Smart Grid*, vol. 2, no. 4, pp. 697–706, Dec. 2011.

[23] S. D. J. McArthur, E. M. Davidson, V. M. Catterson, A. L. Dimeas, N. D. Hatziargyriou, F. Ponci, and T. Funabashi, "Multi-agent systems for power engineering applications—Part I: Concepts, approaches, and technical challenges," *IEEE Trans. Power Syst.*, vol. 22, no. 4, pp. 1743–1752, Nov. 2007.

[24] A. Olshevsky and J. N. Tsitsiklis, "A lower bound for distributed averaging algorithms on the line graph," *IEEE Trans. Autom. Control*, vol. 56, no. 11, pp. 2694–2698, Nov. 2011.

[25] B. Kailkhura, S. Brahma, and P. K. Varshney, "Data falsification attacks on consensus-based detection systems," *IEEE Trans. Signal Inf. Process. Netw.*, vol. 3, no. 1, pp. 145–158, Mar. 2017.

[26] M. Kriegleder, R. Oung, and R. D'Andrea, "Asynchronous implementation of a distributed average consensus algorithm," in *Proc. IEEE/RSJ Int. Conf. Intell. Robots Syst.*, Nov. 2013, pp. 1836–1841.

[27] K. Yu, Q. Ai, S. Wang, J. Ni, and T. Lv, "Analysis and optimization of droop controller for microgrid system based on small-signal dynamic model," *IEEE Trans. Smart Grid*, vol. 7, no. 2, pp. 695–705, Mar. 2016.

[28] N. Pogaku, M. Prodanovic, and T. C. Green, "Modeling, analysis and testing of autonomous operation of an inverter-based microgrid," *IEEE Trans. Power Electron.*, vol. 22, no. 2, pp. 613–625, Mar. 2007.

DEMIN LI (Graduate Student Member, IEEE) received the B.S. and M.S. degrees in electrical engineering from the Hefei University of Technology, Hefei, China, in 2013 and 2016, respectively. He is currently pursuing the Ph.D. degree with the School of Electrical Engineering, Southeast University, Nanjing, China. His research interests include distributed control and microgrid.

ZAIJUN WU (Member, IEEE) received the B.Eng. degree in power system and its automation from the Hefei University of Technology, Hefei, China, in 1996, and the Ph.D. degree in electrical engineering from Southeast University, Nanjing, China, in 2004. He was a Visiting Scholar with the Ohio State University, USA, from 2012 to 2013. He is currently a Professor with the School of Electrical Engineering, Southeast University. He is the author or coauthor of more than 100 refereed journal articles, and a reviewer of several journals. His research interests include microgrid, active distribution network, and power quality.

BO ZHAO (Member, IEEE) received the Ph.D. degree from the Department of Electrical Engineering, Zhejiang University, Hangzhou, China, in 2005. He is currently a Senior Engineer with the State Grid Zhejiang Electric Power Research Institute, Hangzhou, China. His research interests include distributed generation and microgrids.

LEIQI ZHANG (Member, IEEE) received the B.Eng. and Ph.D. degrees from the College of Electrical Engineering, Zhejiang University, Hangzhou, China, in 2012 and 2017, respectively. He is currently an Engineer with the State Grid Zhejiang Electric Power Research Institute, China. His research interest includes distributed generation and control.